Journal of Power Sources 196 (2011) 1530–1536

Contents lists available at ScienceDirect

Journal of Power Sources

journal homepage: www.elsevier.com/locate/jpowsour

Fused ring and linking groups effect on overcharge protection for lithium-ion batteries☆

Wei Weng[a], Zhengcheng Zhang[a,*], Paul C. Redfern[a], Larry A. Curtiss[a,b,c], Khalil Amine[a,**]

[a] Chemical Sciences and Engineering Division, Argonne National Laboratory, 9700 South Cass Avenue, Argonne, IL 60439, USA
[b] Materials Science Division, Argonne National Laboratory, 9700 South Cass Avenue, Argonne, IL 60439, USA
[c] Center for Nanoscale Materials, Argonne National Laboratory, 9700 South Cass Avenue, Argonne, IL 60439, USA

ARTICLE INFO

Article history:
Received 16 July 2010
Received in revised form 16 August 2010
Accepted 17 August 2010
Available online 26 August 2010

Keywords:
Redox shuttle
Overcharge protection
Electrolyte additives
Benzodioxole

ABSTRACT

The derivatives of 1,3-benzodioxan (DBBD1) and 1,4-benzodioxan (DBBD2) bearing two *tert*-butyl groups have been synthesized as new redox shuttle additives for overcharge protection of lithium-ion batteries. Both compounds exhibit a reversible redox wave over 4 V vs Li/Li^+ with better solubility in a commercial electrolyte (1.2 M $LiPF_6$ dissolved in ethylene carbonate/ethyl methyl carbonate (EC/EMC 3/7) than the di-*tert*-butyl-substituted 1,4-dimethoxybenzene (DDB). The electrochemical stability of DBBD1 and DBBD2 was tested under charge/discharge cycles with 100% overcharge at each cycle in MCMB/$LiFePO_4$ and $Li_4Ti_5O_{12}$/$LiFePO_4$ cells. DBBD2 shows significantly better performance than DBBD1 for both cell chemistries. The structural difference and reaction energies for decomposition have been studied by density functional calculations.

1. Introduction

Overcharge abuse has been proposed as one of the common failure mechanisms for lithium-ion batteries [1–3]. Overcharging lithium-ion cells can cause the decomposition of electrode materials, rate acceleration of the irreversible chemical and electrochemical reactions between battery components and rapid increase of the cell temperature. In extreme cases, the voltage runaway can lead to fire hazard and possible explosion. Redox shuttle electrolyte additives have been considered as one of the most economic and convenient solutions to provide overcharge protection as well as auto balancing of the cells in series-connected batteries [4]. In the working hypothesis, the redox shuttle molecule (S) will lose one electron to form a cation radical (S^+) at an intrinsic potential that depends on the nature of the compound. The oxidized form of the shuttle compound will diffuse to the negative electrode to obtain one electron and get reduced. The reversible redox couple S/S^+ thus shuttles the extra charge put into the battery between the electrodes at a defined voltage.The ideal redox shuttle for lithium-ion batteries should meet the following essential requirements: (1) the reversible redox potential of the shuttle molecules should be 0.3–0.4 V higher than the normal operating potential of the positive electrode and (2) the shuttle molecule should be electrochemically stable enough to withstand hundreds of hours of overcharging [4]. These two strict selection criteria have made finding of an excellent redox shuttle extremely challenging. A lot of interesting candidates including metal containing compounds such as ferrocene and ferrocene derivatives [4], neutral radicals such as TEMPO (2,2,6,6-tetramethylpiperinyl-oxides) [5,6] and aromatic organic compounds such as DDB (2,5-di-*tert*-buyl-1,4-dimethoxybenzene) [7–10] and 2-(pentafluorophenyl)-tetrafluoro-1,3,2-benzodioxaborole (PFPTFBDB) [11] have been screened and tested in the open literature.

The general rules of thumb are: (1) aromaticity can enhance the thermodynamic stability of the redox shuttle. In an aromatic system, the positive charge on the oxidized form of shuttle molecule can be delocalized across the π orbitals to maintain conjugation. For example, Dahn et al. [6] concluded two methoxy groups on a benzene ring are necessary according to the $4n+2$ rule for extending the aromatic system along one symmetry axis. (2) The redox shuttle molecule should also have high reaction barriers toward undesired decomposition pathways which are usually initiated by the cleavage the C–H bonds on a benzene ring. The kinetic stability can be enhanced either by introduction of bulky protection groups (i.e. *tert*-butyl) or replacing the C–H bonds with more stable C–F bonds. (3) The reversible redox potentials are sensitive to the substituents. Electron-withdrawing groups make the redox poten-

☆ The submitted manuscript has been created by UChicago Argonne, LLC, Operator of Argonne National Laboratory ("Argonne"). Argonne, a U.S. Department of Energy Office of Science laboratory, is operated under Contract No. DE-AC02-06CH11357. The U.S. Government retains for itself, and others acting on its behalf, a paid-up nonexclusive, irrevocable worldwide license in said article to reproduce, prepare derivative works, distribute copies to the public, and perform publicly and display publicly, by or on behalf of the Government.

* Corresponding author. Tel.: +1 630 252 7868; fax: +1 630 872 4440.
** Corresponding author. Tel.: +1 630 252 3838; fax: +1 630 972 4672.
E-mail addresses: zzhang@anl.gov (Z. Zhang), amine@anl.gov (K. Amine).

0378-7753/$ – see front matter © 2010 Elsevier B.V. All rights reserved.
doi:10.1016/j.jpowsour.2010.08.049

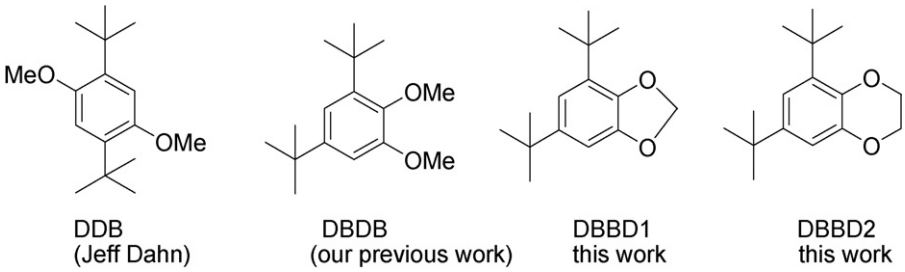

Fig. 1. Chemical structure of non-fused and fused aromatic compounds.

tial more positive and electron donating groups make the redox potential more negative.

DDB (Fig. 1) is one of the organic aromatic compounds that have shown promising results. DDB has an oxidation potential at 3.96 V vs Li/Li^+ and good stability to survive more than 200 overcharge cycles [7,8]. However, the symmetric structure of DDB makes the compound non-polar and it has very limited solubility in polar carbonate solvents. In our recent study, we synthesized DBDB (3,5-di-*tert*-butyl-1,2-dimethoxybenzene, structure is shown in Fig. 1) as one of the non-symmetric isomers of DDB and did a comparative study on its electrochemical properties in overcharging conditions [12]. DBDB exhibits much better solubility in commercial electrolyte, but significantly poorer stability. Based on our experimental data and density functional results, we postulated that the conformation of two alkoxy bonds in DDB and DBDB is the key factor affecting their electrochemical stability. In DBDB, one methoxy group is in the plane of benzene ring, the other methoxy group points out of the ring due to the formation of an intramolecular hydrogen bond between the C–H of the *tert*-butyl group and the oxygen of the methoxyl group. The deviation from a coplanar geometry of this other methoxy group and the benzene ring reduces the P–π conjugation efficiency in DBDB. We also found that the radical DDB cation was likely stable to decomposition due to a large activation barrier.

Here, we describe the synthesis of 1,3-benzodioxan (DBBD1) and 1,4-benzodioxan (DBBD2) derivatives incorporating a side fused ring structure. Their electrochemical stability under overcharge condition has been evaluated. The effect of the fused heterocycle structure and the length of the linking groups has been discussed and analyzed by density functional calculations.

2. Experimental

4,6-Di-*tert*-butyl-1,3-benzodioxole (DBBD1) and 5,7-di-*tert*-butyl-1,4-benzodioxin (DBBD2) are not commercially available. The synthesis of DBBD1 and DBBD2 has been previously reported by Kashima et al. [13]. However, the compounds have not been fully characterized.

^1H and ^{13}C NMR experiments were performed on a Bruker model DMX 500 NMR spectrometer (11.7 T).

Synthesis of DBBD1: 3,5-di-*tert*-butylhydroquinone (6.7 g) was dissolved in CH_2Cl_2 (300 mL). Triethylbenzylammonium chloride (6.8 g, 30 mmol) and aqueous sodium hydroxide aqueous solution (100 mL, 30%) was added to the previous solution. The reaction was stirred at ambient temperature overnight. The organic layer was separated, washed with water and dried over $MgSO_4$. The resulting solution was concentrated to afford a crude oil. The crude product was chromatographed (silica, hexane/ethyl acetate (20/1)) mixture to afford the pure compound (R_f = 0.5, 10:1 hexane/ethyl acetate). Yield: 50%. ^1H NMR (500 MHz, $CDCl_3$): δ 6.79 (m, 2H), 5.90 (s, 2H, $-OCH_2O-$), 1.35 (s, 9H, CMe_3), 1.23 (s, 9H, CMe_3). ^{13}C (125 MHz, $CDCl_3$): δ 147.4, 144.5, 142.5, 131.8, 115.3, 104.2, 99.9 ($-OCH_2O-$), 34.8 (CMe_3), 34.0 (CMe_3), 31.7 (CMe_3), 29.5 (CMe_3).

Synthesis of DBBD2: 3,5-di-*tert*-butylhydroquinone (3.33 g) was mixed with 1,2-di-bromoethane (5.6 g), potassium carbonate (4.35 g) and ethylene glycol (25 mL). The mixture was heated in a 120 °C oil bath under the protection of Argon gas for 12 h. Water was added to the reaction mixture to quench the reaction and then the organic compound was extracted by CH_2Cl_2. The resulting solution was concentrated to afford a crude oil. The crude product was chromatographed (silica, hexane/ethyl acetate 20/1) mixture to afford the pure compound (R_f = 0.5, 5:1 hexane/ethyl acetate). Yield: 60%. ^1H NMR (500 MHz, $CDCl_3$): δ 7.03 (d, J = 2 Hz, 1H), 6.93 (d, J = 2 Hz, 1H), 4.34 (s, 4H, $-OCH_2CH_2O-$), 1.53 (s, 9H, CMe_3), 1.43 (s, 9H, CMe_3). ^{13}C (125 MHz, $CDCl_3$): δ 142.9, 139.9, 137.8, 115.6, 112.3, 64.0 ($-OCH_2CH_2O-$), 63.4 ($-OCH_2CH_2O-$), 35.0 (CMe_3), 34.3 (CMe_3), 31.5 (CMe_3), 29.7 (CMe_3).

Cyclic voltammetry experiments using a Solartron Analytical 1470E system were performed in custom-made three-electrode cells with a 1.6-mm diameter Pt working electrode, a Li reference electrode, and a Li counter electrode. The electrolyte tested was 1.2 M $LiPF_6$ in a mixture of ethylene carbonate and ethyl methyl carbonate (EC/EMC) in a volume ratio of 3/7. The DBBD1 and DBBD2 shuttle molecules were added to the electrolyte in a concentration of 0.1 M. The sweep rate was varied from 10 to 200 mV/s.

Overcharge tests were conducted in 2032 coin-type cells of $Li_4Ti_5O_{12}/LiFePO_4$ or MCMB/$LiFePO_4$. The electrolyte was 1.2 M $LiPF_6$ in EC/EMC 3/7 containing 0.2 M DBBD1 or DBBD2. The cells were charged at a constant current to 200% of their normal capacity (100% overcharge) or until a specific upper cutoff voltage was reached (normally 4.95 V vs Li/Li^+), whichever occurred first. After overcharging, the cells were discharged using the same constant current.

3. Results and discussion

3.1. Synthesis and characterization

Fig. 2 shows the synthesis of DBBD1 and DBBD2 from commercially available starting material 3,5-di-*tert*-butylcatechol. ^1H NMR (Fig. 3) of both products exhibits characteristic signals for the linking methylene group. The two CH_2 groups in DBBD2 are not equivalent, but their ^1H NMR resonance signals are accidentally coincident. However, ^{13}C NMR resonance signals for two CH_2 groups in DBBD2 are well-resolved indicating the different environment around the methylene carbons. The CH_2 linkage of DBBD1 exhibits much more downfield chemical shift in ^1H and ^{13}C NMR than the CH_2CH_2 linkage of DBBD2 (^1H NMR: 5.9 vs 4.34; ^{13}C NMR: 99.9 vs 64 and 63.4). The NMR data also confirmed the presence of two non-equivalent *tert*-butyl groups in each compound.

DBBD1 and DBBD2 have lower symmetry and larger dipole moments than DDB. They have good solubility in carbonate-based electrolyte. Similar to DBDB, high concentration solutions (1.0 M) of DBBD1 and DBBD2 in 1.2 M $LiPF_6$ EC/EMC 3/7 can be prepared.

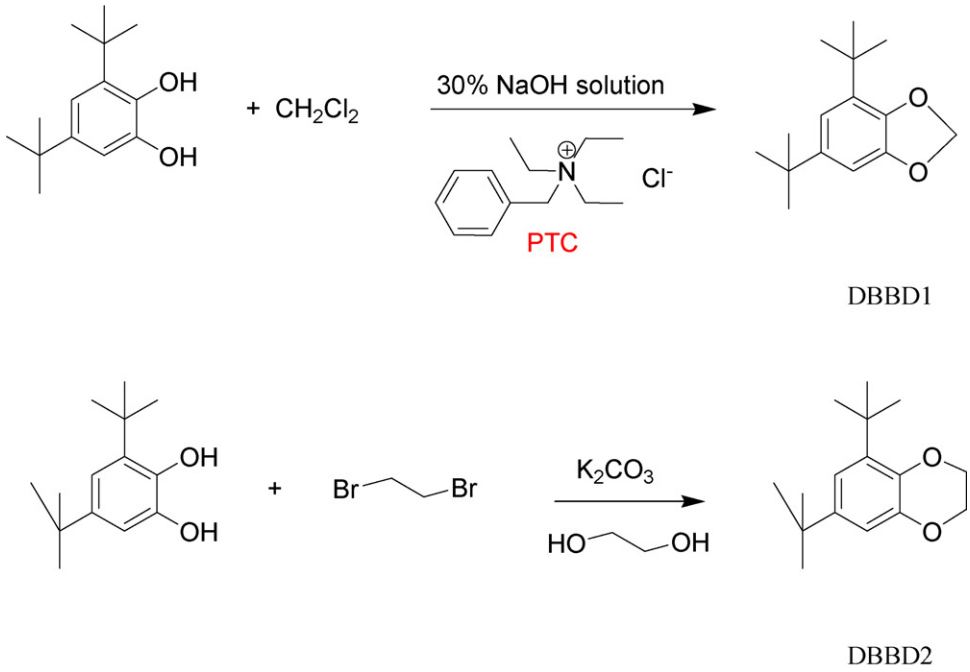

Fig. 2. Synthesis of DBBD1 and DBBD2.

3.2. Electrochemical measurements

Figs. 4 and 5 show cyclic voltammograms for 0.1 M DBBD1 and DBBD2 dissolved in 1.2 M $LiPF_6$ EC/EMC (3/7) electrolytes with sweep rate of 10, 20, 50, 100 and 200 mV s^{-1}. Both compounds display a well-defined reversible redox wave. The standard redox potential, evaluated using the average of the anodic and cathodic potentials $(E_a + E_p)/2$, is 4.12 V (DBBD1) and 4.17 V (DBBD2) vs Li/Li^+, which is about 0.2 V higher than that of DDB (3.92 V). Usually the introduction of an electron-withdrawing group increases the redox potential of the parent molecule. Our observations showcases that the fused ring structure also affects the redox potential.

The diffusion coefficient of DBBD1 and DBBD2 has been determined by plotting the anodic peak current (I_p) versus the square root of the sweep rates ($\nu^{1/2}$). Data is analyzed according to the Randles–Sevcik equation (Eq. (1)) [9], where I_p is the anodic peak current, n is the number of electrons involved in the redox process, C is the concentration of redox shuttle and D is the diffusion coefficient.

$$I_p = 2.69 \times 10^5 n^{3/2}\ AD^{1/2}\ \nu^{1/2} C \quad (1)$$

The plot of I_p vs $\nu^{1/2}$ is quite linear for DBBD1 and DBBD2 as shown in Fig. 6, which suggests diffusion-controlled redox chemistry. The diffusion coefficient in 1.2 M $LiPF_6$ EC/EMC electrolyte was determined to be 1.4×10^{-6} $cm^2\ s^{-1}$ for DBBD1 and 1.7×10^{-6} $cm^2\ s^{-1}$ for DBBD2. These values are comparable to what is observed for DDB (1.6×10^{-6} $cm^2\ s^{-1}$) and DBDB (1.63×10^{-6} $cm^2\ s^{-1}$). This can be explained by the structural similarity of these four compounds.

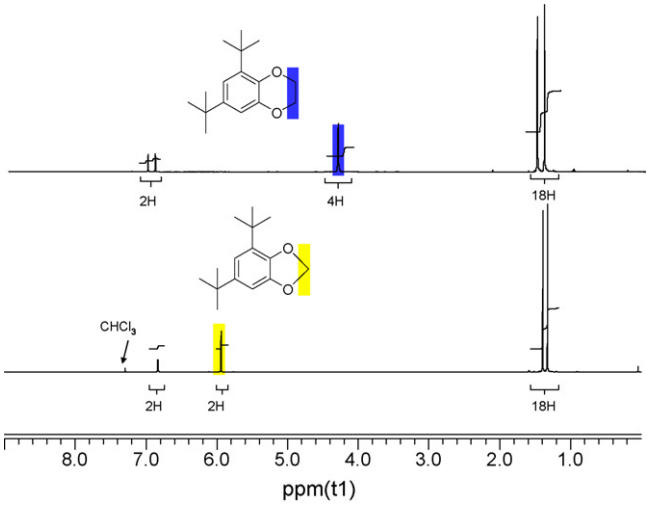

Fig. 3. Stacked ^1H NMR spectra of DBBD1 and DBBD2 in $CDCl_3$.

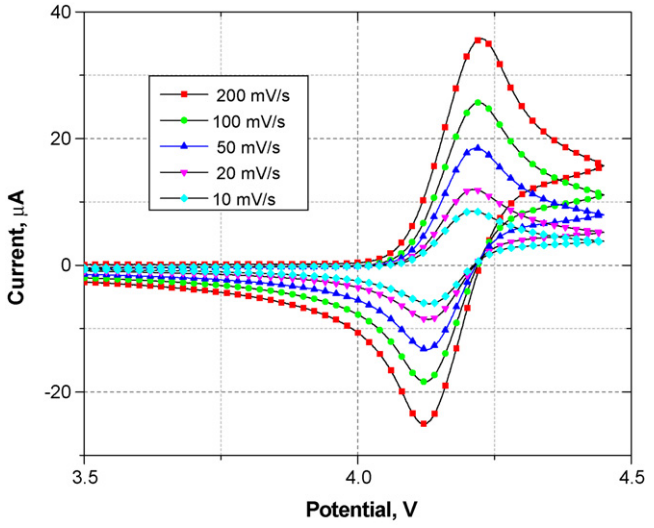

Fig. 4. Cyclic voltamograms of 0.1 M DBBD1 in 1.2 M $LiPF_6$ EC/EMC (3/7 V/V) using a Pt/Li/Li three-electrode cell.

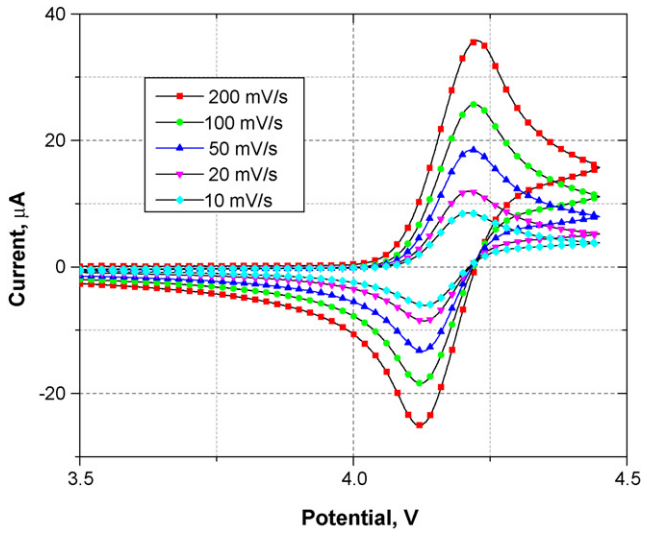

Fig. 5. Cyclic voltamograms of 0.1 M DBBD2 in 1.2 M $LiPF_6$ EC/EMC (3/7 V/V) using a Pt/Li/Li three-electrode cell.

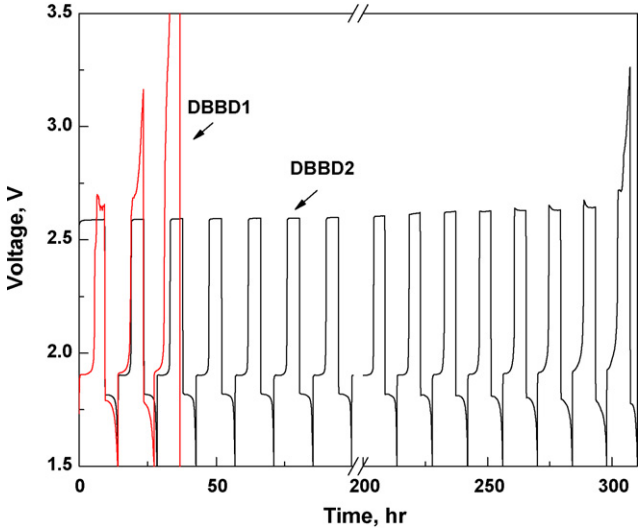

Fig. 7. Voltage profiles of $Li_4Ti_5O_{12}$/$LiFePO_4$ cells containing 0.2 M DBBD1 or DBBD2 during the overcharge tests (*C*/5 charging rate, time axis breaks between 100 and 200 h).

3.3. Overcharge tests of DBBD1 and DBBD2 in $Li_4Ti_5O_{12}$/$LiFePO_4$ cells

Fig. 7 shows the voltage profiles of $Li_4Ti_5O_{12}$/$LiFePO_4$ cells containing 0.2 M DBBD1 and 0.2 M DBBD2 in 1.2 M $LiPF_6$ in the EC/EMC electrolyte using a *C*/5 charging rate. The cells were first cycled between 2 and 0.5 V with a constant current of *C*/10 (not shown in Fig. 7) as a formation step before they were charged to 2.8 mAh (100% overcharge) or until 4.95 V. The cell with DBBD2 was at 100% SOC before the overcharge test, while the cell with DBBD1 was at fully discharged state. Therefore, in the first overcharge cycle, the cell with DBBD2 was actually 200% overcharged and the cell with DBBD1 was normally 100% overcharged. After the first overcharge cycle, the normal charging plateau appeared at 1.9 V vs $Li_4Ti_5O_{12}$ and the cells were charged to full capacity in about 5 h. Further charging increased the voltage of the cells until the redox potential of redox shuttles were reached, at which point the second charging plateau was observed at 2.6 V vs $Li_4Ti_5O_{12}$ (4.1 V vs Li/Li^+). The cells were overcharged for another 5 h and then discharged. In this test DBBD2 shows significantly better stability than DBBD1. DBBD2 can withstand more than 20 overcharge cycles, whereas DBBD1 starts to display uncontrolled voltage increase in the third cycle.

Fig. 8 shows the charge/discharge capacity of these two testing cells. DBBD2 is able to provide overcharge protection and flat discharge capacity for more than 20 cycles. However, DBBD1 showed much poorer performance; the cell starts to lose its capacity even at the second cycle.

Fig. 9 shows the voltage profile of $Li_4Ti_5O_{12}$/$LiFePO_4$ 2302 cells containing a low concentration (0.1 M) of DBBD2 using a lower current (*C*/10) for the overcharge test with 100% overcharge. In this mild test condition, the DBBD2 shuttle can provide an extended overcharge protection of 42 cycles.

3.4. Overcharge tests of DBBD1 and DBBD2 in MCMB/$LiFePO_4$ cells

Fig. 10 shows the voltage profile of MCMB/$LiFePO_4$ cells containing 0.2 M DBBD1 or DBBD2 as redox shuttles cycling at *C*/5 with

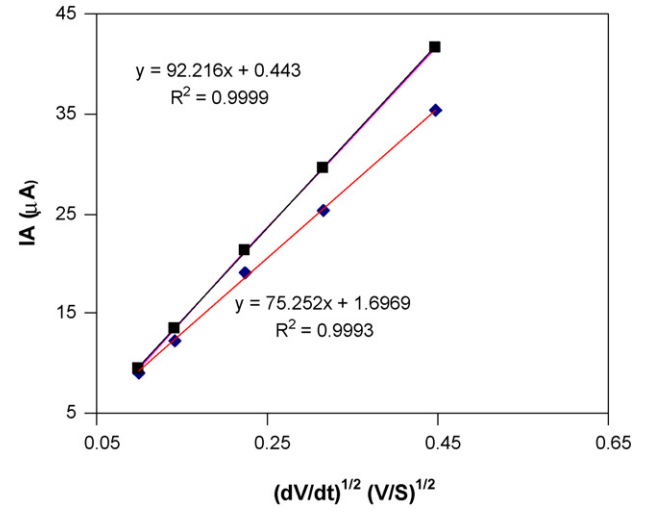

Fig. 6. Plots of I_p vs the square root of the sweep rate (DBBD1: red line; DBBD2: black line). (For interpretation of the references to color in this figure legend, the reader is referred to the web version of this article.)

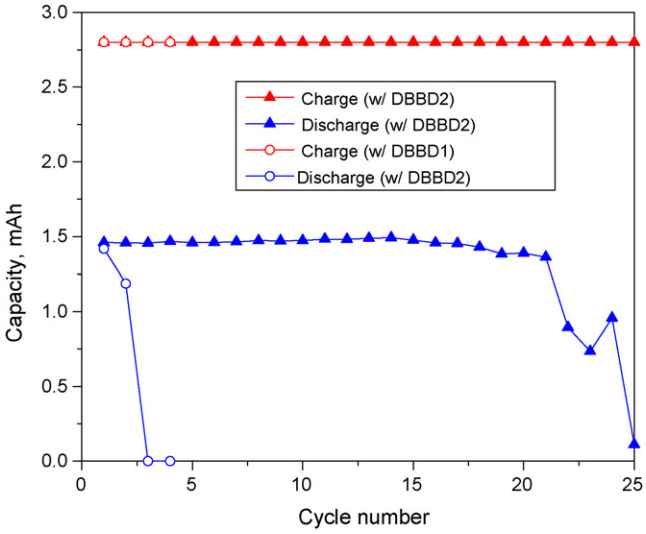

Fig. 8. Charge and discharge capacity of the $Li_4Ti_5O_{12}$/$LiFePO_4$ cells containing 0.2 M DBBD1 or DBBD2 during the overcharge test (*C*/5 charging rate).

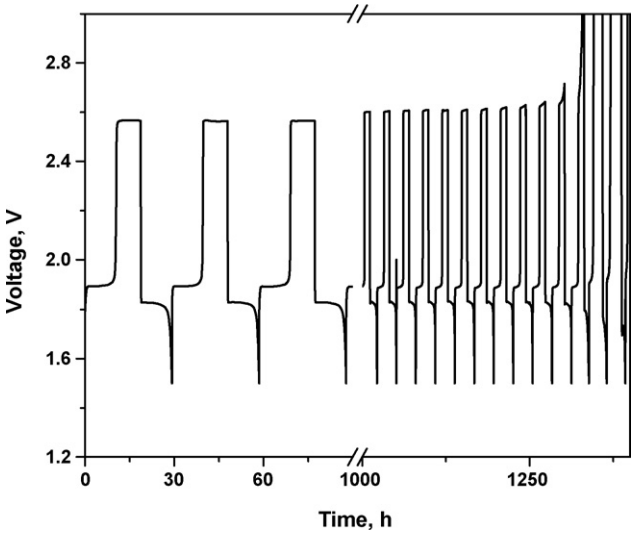

Fig. 9. Voltage profiles of $Li_4Ti_5O_{12}$/$LiFePO_4$ cells containing 0.1 M DBBD2 during the overcharge tests (*C*/10 charging rate, Time axis breaks between 90 and 1000 h).

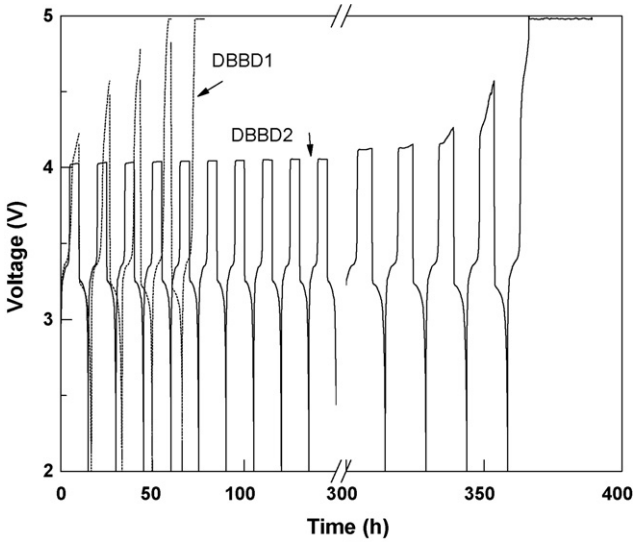

Fig. 10. Voltage profiles of MCMB/$LiFePO_4$ cells containing 0.2 M DBBD2 during the overcharge tests (*C*/5 charging rate, time axis breaks between 150 and 300 h).

100% overcharge. The normal charge took place at about 3.4 V. After the full capacity was attained, the cell voltage went up rapidly until the plateau of shuttle was reached (4.03 V). DBBD2 was able to survive 24 cycles at 100% overcharge condition, however, DBBD1 can only afford 1 cycle.

3.5. Density functional theory results on a possible failure mechanism

As illustrated in Fig. 1, DBBD1 and DBBD2 have similar molecular structures. Both compounds contain a heterocyclic ring with two oxygen atoms fused to a *tert*-butyl-substituted benzene ring. They have similar redox potentials as well as diffusion coefficients. Interestingly, one extra CH_2 spacer between the two oxygen atoms in DBBD2 significantly improved its electrochemical sta-

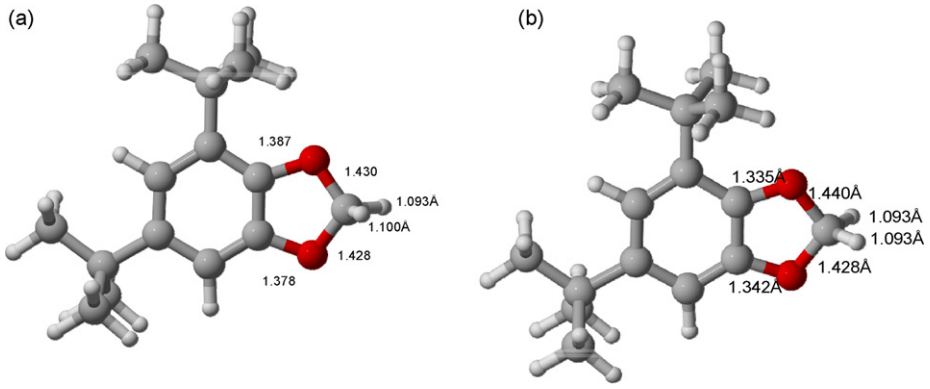

Fig. 11. B3LYP/631G* optimized geometries of (a) neutral DBBD1 and (b) DBBD1 radical cation.

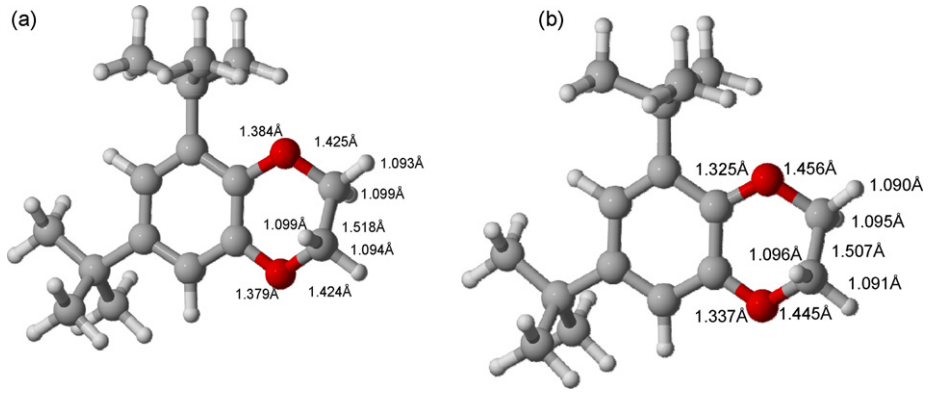

Fig. 12. B3LYP/631G* optimzed geometries of (a) neutral DBBD2 and (b) DBBD2 radical cation.

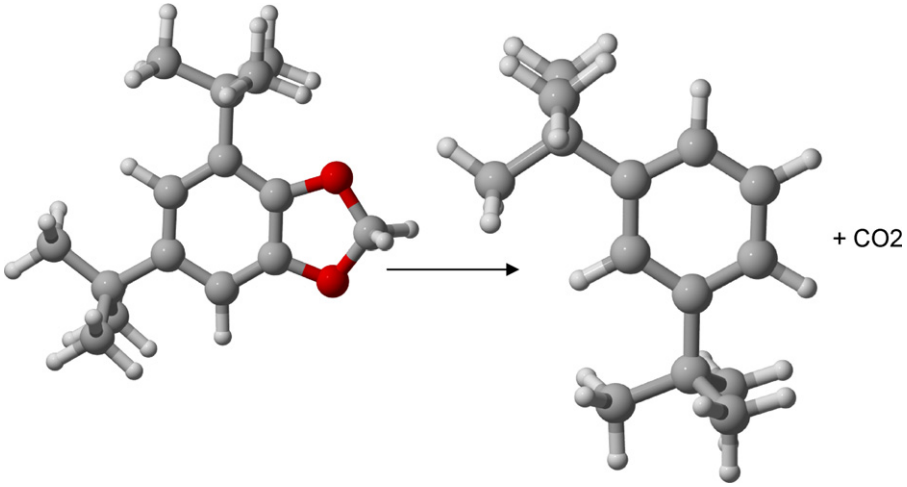

Fig. 13. Decomposition of DBBD1 radical cation to form *meta*-di-*tert*-butylbenzene cation and CO_2.

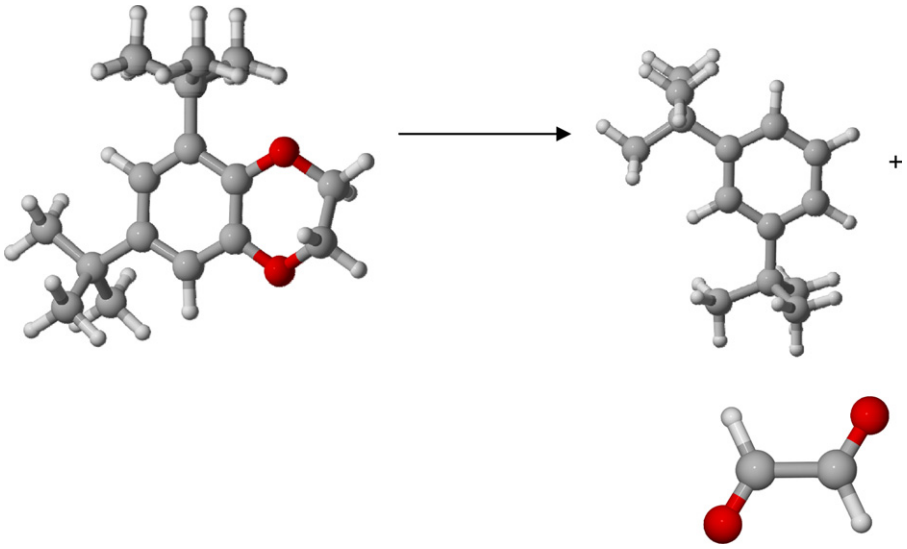

Fig. 14. Decomposition of DBBD2 radical cation to form ethanedial and *meta*-di-*tert*-butylbenzene cation.

bility over DBBD1. We have used density functional theory to optimize the structures of the two molecules, calculate their oxidation potentials, and determine the thermodynamics for possible decomposition pathways using density functional theory.

All structures were optimized with the B3LYP/6-31G* method [14,15]. This was followed by calculation of free energies at 298 K including salvation free energies from B3LYP/631+G* calculations at the B3LYP/631G* geometries using the PCM continuum model with water solvent modified to have a dielectric constant (ε) of 55.7, which represents a solvent composed of 25% ethylene carbonate/25% ethyl methyl carbonate/50% propylene carbonate [16]. Finally, larger basis set effects were taken into account with single point B3LYP/6311+G(3df,2p) calculations. The resulting energies were used to calculate free energies for possible decomposition reactions and to calculate oxidation potentials. The latter were adjusted to be relative to the Li/Li^+ reference electrode by subtracting 1.46 V from the resulting value. These methods should give a reasonably accurate account of the reaction energies [17–19]. All calculations were performed using the Gaussian 03 code [15].

The optimized structures of the neutral species DBBD1 and DBBD2 and their radical cations are shown in Figs. 11 and 12. The calculated oxidation potentials of the neutral species are 4.05 and 4.08 V, respectively. This is in good agreement with the experimental values of 4.12 and 4.17 V. We calculated the reaction free energies in solution at 298 K of several likely decomposition pathways for oxidized DBBD1 and DBBD2 species. One way that the DBBD1 radical cation can decompose is by forming CO_2 and *meta*-di-*tert*-butylbenzene cation as shown in Fig. 13. The decomposition reaction of the DBBD1 cation radical is exothermic by 1.5 eV. In contrast, the DBBD2 radical cation can decompose to form *meta*-di-*tert*-butylbenzene cation and ethanedial (glyoxal) (Fig. 14), which is endothermic by 0.2 eV. This suggests that the DBBD2 shuttle is more stable than the DBBD1 shuttle, which is in good agreement with the experimental results.

4. Conclusions

Two benzodioxan derivatives DBBD1 and DBBD2 are synthesized and studied as new redox shuttle additives. These new shuttle molecules have much better solubility in the conventional carbonate-based electrolyte than DDB. Overcharging test results indicated that the one extra CH_2 spacer in DBBD2 can greatly enhance its electrochemical stability compared to DBBD1. DBBD2 displayed slightly improved stability over DBDB reported previously by our group; however as asymmetric derivatives of DDB,

both DBBD1 and DBBD2 are more prone to decomposition under overcharge conditions. Density functional calculations suggest the formation of CO_2 as the decomposition product of DBBD1 is the driving force for its fast decomposition under overcharge conditions.

References

[1] T. Ohsaki, T. Kishi, T. Kuboki, N. Takami, N. Shimura, Y. Sato, M. Sekino, A. Satoh, J. Power Sources 146 (2005) 97.
[2] R.A. Leising, M.J. Palazzo, E.S. Takeuchi, K.J. Takeuchi, J. Electrochem. Soc. 148 (2001) A838.
[3] R.A. Leising, M.J. Palazzo, E.S. Takeuchi, K.J. Takeuchi, J. Power Sources 97–98 (2001) 681.
[4] Z. Chen, Y. Qin, K. Amine, Electrochim. Acta 54 (2009) 5605.
[5] M. Taggougui, B. Carr, P. Willmann, D. Lemordant, J. Power Sources 174 (2007) 643.
[6] C. Buhrmester, J. Chen, L. Moshurchak, J. Jiang, R.L. Wang, J.R. Dahn, J. Electrochem. Soc. 152 (2005) A2390.
[7] C. Buhrmester, J. Chem, L. Moshurchak, J.W. Jiang, R.L. Wang, J.R. Dahn, J. Electrochem. Soc. 152 (2005) A2390.
[8] J. Chen, J.R. Dahn, Electrochem. Solid-State Lett. 8 (2005) A59.
[9] J.K. Feng, X.P. Ai, Y.L. Cao, H.X. Yang, Electrochem. Commun. 9 (2007) 25.
[10] L.M. Moshuchak, M. Bulinski, W.M. Lamanna, R.L. Wang, J.R. Dahn, Electrochem. Commun 9 (2007) 1497.
[11] Z. Chen, K. Amine, Electrochem. Commun. 9 (2007) 703.
[12] Z. Zhang, L. Zhang, J.A. Schlueter, P.C. Redfern, L. Curtiss, K. Amine, J. Power Sources 195 (2010) 4957.
[13] C. Kashima, A. Tomotake, Y. Omote, J. Org. Chem. 52 (1987) 5616.
[14] A.D. Becke, J. Chem. Phys. 98 (1993) 5648.
[15] M.J. Frisch, G.W. Trucks, H.B. Schlegel, G.E. Scuseria, M.A. Robb, J.R. Cheeseman, J.A. Montgomery Jr., T. Vreven, K.N. Kudin, J.C. Burant, J.M. Millam, S.S. Iyengar, J. Tomasi, V. Barone, B. Mennucci, M. Cossi, G. Scalmani, N. Rega, G.A. Petersson, H. Nakatsuji, M. Hada, M. Ehara, K. Toyota, R. Fukuda, J. Hasegawa, M. Ishida, T. Nakajima, Y. Honda, O. Kitao, H. Nakai, M. Klene, X. Li, J.E. Knox, H.P. Hratchian, J.B. Cross, V. Bakken, C. Adamo, J. Jaramillo, R. Gomperts, R.E. Stratmann, O. Yazyev, A.J. Austin, R. Cammi, C. Pomelli, J.W. Ochterski, P.Y. Ayala, K. Morokuma, G.A. Voth, P. Salvador, J.J. Dannenberg, V.G. Zakrzewski, S. Dapprich, A.D. Daniels, M.C. Strain, O. Farkas, D.K. Malick, A.D. Rabuck, K. Raghavachari, J.B. Foresman, J.V. Ortiz, Q. Cui, A.G. Baboul, S. Clifford, J. Cioslowski, B.B. Stefanov, G. Liu, A. Liashenko, P. Piskorz, I. Komaromi, R.L. Martin, D.J. Fox, T. Keith, M.A. Al-Laham, C.Y. Peng, A. Nanayakkara, M. Challacombe, P.M.W. Gill, B. Johnson, W. Chen, M.W. Wong, C. Gonzalez, J.A. Pople, Gaussian 03, Revision C.02, Gaussian, Inc., Wallingford, CT, 2004.
[16] J.M. Vollmer, L.A. Curtiss, D.R. Vissers, Khalil Amine, J. Electrochem. Soc. 151 (1) (2004) A178.
[17] L.A. Curtiss, K. Raghavachari, P.C. Redfern, J.A. Pople, J. Chem. Phys. 106 (1997) 1063.
[18] L.A. Curtiss, P.C. Redfern, K. Raghavachari, J.A. Pople, J. Chem. Phys. 109 (1998) 42.
[19] L.A. Curtiss, P.C. Redfern, K. Raghavachari, J. Chem. Phys. 123 (2005) 124107.